www.elsevier.com/locate/memsci

NANOFILTRATION SEPARATION OF POLYVALENT AND MONOVALENT ANIONS IN DESALINATION BRINES

A. Pérez-González, R. Ibáñez, P. Gómez, A.M. Urtiaga, I. Ortiz, J.A. Irabien

PII: S0376-7388(14)00669-3
DOI: http://dx.doi.org/10.1016/j.memsci.2014.08.045
Reference: MEMSCI13157

To appear in: *Journal of Membrane Science*

Received date: 23 May 2014
Revised date: 20 August 2014
Accepted date: 24 August 2014

Cite this article as: A. Pérez-González, R. Ibáñez, P. Gómez, A.M. Urtiaga, I. Ortiz, J.A. Irabien, NANOFILTRATION SEPARATION OF POLYVALENT AND MONOVALENT ANIONS IN DESALINATION BRINES, *Journal of Membrane Science*, http://dx.doi.org/10.1016/j.memsci.2014.08.045

NANOFILTRATION SEPARATION OF POLYVALENT AND MONOVALENT ANIONS IN DESALINATION BRINES

A. Pérez-González[a], R. Ibáñez[a], P. Gómez[b], A.M. Urtiaga[a], I. Ortiz[a,*], J.A. Irabien[a]

[a]Chemical and Biomolecular Engineering Department. Universidad de Cantabria, Avda. de los Castros s/n, 39005 Santander, Spain

[b]APRIA Systems S.L., Polígono Trascueto, s/n, 29600 Camargo, Cantabria, Spain. consultec@apriasystem.es

*Corresponding author

Tel.: +34 942 20 15 85; fax: +34 942 20 15 91.

E-mail address: ortizi@unican.es

ABSTRACT

This work, as part of a global membrane process for the recovery of alkali and acids from reverse osmosis (RO) desalination brines, focuses on the nanofiltration (NF) separation of polyvalent and monovalent anions, more specifically sulfate and chloride. This pretreatment stage plays a key role in the whole recovery process. Working with model brines simulating the concentration of RO concentrates, 0.2-1.2M chloride concentration and 0.1M sulfate concentration, the experimental performance and modeling of the NF separation is reported. The study has been carried out with the NF270 (Dow Filmtec) membrane. The effect of operating pressure (500-2000 kPa), ionic strength (0.4-1.3 M) and chloride initial concentration (0.2-1.2 M) on the membrane separation capacity has been investigated. Finally, the Donnan Steric Pore Model (DSPM) together with experimentally determined parameters: effective pore radius (r_p); thickness of the membrane effective layer (δ) and effective membrane charge density (X_d), was proved accurate enough to satisfactorily describe the experimental results. In this work we provide for the first time the analysis of partitioning effects and transport mechanism in the NF separation of sulfate and chloride anions in concentrations that simulate those found in RO desalination brines.

Keywords

Desalination brines; Nanofiltration; Streaming potential; Separation sulfate/chloride

1. INTRODUCTION

In the context of desalination, RO membrane technology has been developed over the past 40 years, being the leading technology for new desalination installations. Water shortage problems in dry inland regions are increasingly satisfied through RO desalination of brackish groundwater's resources. Exploitation of brackish groundwaters is advantageous due to the lower salt concentration of the inlet water compared to seawater, which reduces the osmotic pressure to be overcome and the energy consumption [1]. However, the management of concentrates is an important drawback because brine discharges from inland installations still remains being a problem with not many feasible alternatives [2]. In coastal desalination plants, brines are directly discharged to the sea, posing adverse environmental effects on the receiving marine environment [3].

Alternatives aiming at zero liquid discharge, through combination of different technologies, are highlighted as the most promising management options [4]. In this work a sequential process based on the appropriate combination of membrane technologies is proposed with the aim of reducing the adverse environmental impact of brine discharge, together with the recovery of valuable products contained in the concentrated brine, namely alkali and acids. The strategy to achieve this goal implies, first, a pretreatment step of the brine to remove scaling salts and impurities, followed by Bipolar Membrane Electrodialysis (BMED) to recover hydrochloric acid (HCl) and sodium hydroxide (NaOH). This technology has proved to be technically feasible for the production of 1.0 M or higher acid and alkali solutions [5].

Thus, this work is focused on the pretreatment stage, specifically on the separation of sulfate from the brine to avoid its negative effects in BMED. For this purpose, NF has been selected and considered a potential and effective alternative.

Nanofiltration is a pressure driven membrane separation process with intermediate separation effectiveness between RO and ultrafiltration (UF). NF membranes are typically polymeric, asymmetric and consist of a low resistance support layer with a functionally active porous top layer [6,7]. NF membranes have properties that combine size and electrical effects. The pores are typically near 1 nm in diameter and have fixed charges. Due to these characteristics, NF membranes retain multivalent complex ions and permeate small uncharged solutes and low charged ions [8-10]. This, along with the small energy consumption of the process and the high fluxes attained, makes NF membranes extremely useful in fractionation and selective removal of solutes from complex process streams [11]. However, the description of membrane NF separations is extremely complex and is dependent on the micro-hydrodynamics and interfacial events occurring at the membrane surface and within the membrane nanopores [12]. There is significant debate as to the exact nature of these complex phenomena, and the rejection is typically attributed to a combination of steric and electrical effects [6]. Modelling of transport through membranes is an essential engineering aspect; although many models for nanofiltration have been proposed by several researchers [13-18], a realistic model that describes rejection of charged molecules has never been well established [19]. Thus, this work investigates experimentally and theoretically the NF separation of sulfate and chloride co-ions from highly concentrated solutions providing the tools needed for the design and optimization of the recovery of brackish and seawater RO desalination brines.

2. EXPERIMENTAL MATERIALS AND METHODS

2.1. Chemical characterization of brines

The salinity of brackish groundwaters water ranges from 1,000 to 8,000 mg/L of total dissolved solids (TDS) while the value for marine water is typically around 35,000 mg/L TDS [20]. However, constituent concentrations in the RO brines are found to be double or higher than in feed water. In this study, RO brines obtained from a brackish water desalination plant (Cuevas de Almanzora) and from two seawater desalination plants (Carboneras and Las Aguilas) located in Spain were taken as reference to set the ionic concentration (Table 1) of model brines used in NF experiments. The concentration of chloride, sulfate and nitrate was determined by ion chromatography (Dionex ICS-1100, Sunnyvale, CA, USA). The concentration of phosphate was determined by the ascorbic acid method according to Standard Methods 4500-PE. The concentration of cations was determined by Inductively coupled plasma - optical emission spectroscopy (ICP-OES) (Perkin Elmer Plasma Emission Spectrometer ICP 400, Connecticut, USA), except for concentration of iron and manganese, which was determined by atomic absorption spectroscopy (AAS) (Perkin Elmer 3110, Connecticut, USA). The pH was measured by using a portable pH-meter (Crison pH 25) and conductivity and TDS with a portable conductivity meter (HACH sesION 5). Hardness was determined by EDTA titrimetric method according to Standard Methods 2340 C. The concentration of carbonates and bicarbonates was measured by titration method according to Standard Method 2320 B.

Given the high ionic concentration of desalination brines of Table 1 it is concluded that any recovery process needs of the separation and purification steps where the valuable compound, chloride in the present case, is separated from other major and

minor components. Alkali precipitation, with partial use of the recovered NaOH in BMED, would be the most suitable option for hardness removal at industrial level. The high concentration of sulfate in the analyzed brines is a consequence of the geological characteristics of the area, rich in gypsum. The experimental part of this study has been carried out using model brines with a fixed sulfate content of 8,000 mg/L (0.1M), the most unfavorable condition for its separation, and chloride concentrations in the range from 5,000 mg/L to 40,000 mg/L (0.2-1.2M) in order to cover the concentration range of brines from brackish water desalination to seawater desalination. Specifically, four synthetic brines with molar ratios chloride/ sulfate: α=1.7, 5.1, 10.2 and 13.6 were prepared in order to evaluate the effect of operating pressure and ionic strength in sulfate and chloride rejection, and also the influence of initial chloride concentration in sulfate rejection was evaluated.

2.2. Streaming potential measurement

The streaming potential was measured with a SurPASS electrokinetic analyzer UAnton (Anton Paar, Barcelona; Spain). All the measurements were carried out at pH 6. Streaming potential is usually measured using as electrolyte KCl solutions in a low concentration range (0.001 to 0.01M) as reported in literature for the membrane NF270 used in this study [21-27]. However, those electrolyte solutions are not representative of the conditions applied in this study during NF operation. So, in this work a somewhat modified procedure was followed based on the fundamentals of surface charge of NF membranes. It is known that a polymeric membrane acquires surface charge when brought into contact with an aqueous medium [28]. Therefore, NF270 membrane samples were immersed in the model brines for 24 hours to allow the active layer to acquire the corresponding charge [29,30]. After this time, the streaming potential was determined using 0.1 M NaCl as electrolyte, that is the

maximum acceptable concentration according to the operating restrictions of the equipment. This experimental protocol was developed to be able to measure the streaming potential established in high saline concentrations as those as the model brines used in this study. Achieved results using this procedure are in good agreement with other studies [31,32] as it will be explained in section 3.1.2.

2.3. Experimental set-up and operation protocol

2.3.1. Experimental membrane set-up

All membrane experiments were carried out in a laboratory test cell using a SEPA-CF (GEOsmonics, France) cross-flow module. The selection of the nanofiltration membrane NF270 (Dow Filmtec) was based on the information given by membrane manufacturers and previous studies reported in the literature [18,19,33]. The membrane area was 0.014 m^2 and total recirculation was used for both the permeate and the concentrate solutions that were returned to the feed reservoir. The feed was pressurized at three pressure values of 500, 1000 and 2000 kPa, and flowed with a cross flow rate value (tangential recirculation of the feed stream) of 2.5 L min^{-1}. The permeate chamber was maintained at atmospheric pressure. The solute concentration in the feed, permeate and concentrate samples was determined by ion chromatography (Dionex ICS-1100, Sunnyvale, CA, USA) provided with an AS9-HC column for the determination of anions and with a CS12A column for the determination of cations.

2.3.2. Operation protocol

New membranes were immersed in deionized water overnight before being used, and then pressurized to 1000 kPa in the nanofiltration module, circulating deionized water for two hours, to avoid any compression effects and to establish leak tightness

[34]. Temperature was controlled using an Advanced Digital Refrigerating/Heating Circulator (Polyscience AD15R-30-A12E) and was maintained constant at 293 K in all experiments. The ions rejection was determined from the difference between the concentration of the ion in the permeate and the concentration of ion in the retentate, according to Eq. (1).

$$\mathcal{R}_i = 1 - \frac{C_{P_i}}{C_{R_i}} \quad (1)$$

For each molar ratio between chloride and sulfate ions (α), three operational pressures: 500, 1000 and 2000 kPa were studied. Samples of feed, retentate and permeate were collected when the steady state was reached, at least one hour after the start-up of each test and for the next two hours. During this experimental period, continuous monitoring and control of the operating parameters such as operating pressure, flow rate, temperature, pH and conductivity of brine solution was undertaken to minimize the experimental error. In order to assure steady state conditions, it was checked that constant volumetric flux and constant ions concentration in the permeate and rejection streams were achieved, by comparing the values in at least three consecutive samples obtained at a given set of experimental conditions. All the experiments were developed at natural pH of solutions (pH=6.3±0.3). Experiments were performed in triplicate (average standard deviation among replica of 0.6%) for all the conditions previously described.

3. RESULTS AND DISCUSSION

3.1. Membrane characterization

3.1.1. SEM analysis

SEM micrographs were taken to determine the thickness of the NF270 membrane effective layer. The NF270 membrane is a thin film composite of polyester support matrix, microporous polysulfone interlayer and polyamide barrier layer, as can be seen in Fig. 1. It is assumed that the thin active layer controls both water and salts fluxes across the membrane and it determines its selectivity and salt rejection [35]. The thickness of the effective layer made up of polyamide, δ=7±0.27 μm, was determined from these SEM images.

The value of membrane pore radius of the NF270 membrane was taken from Lin et al.[24] and Oatley et al. [6], as r_p=0.43 nm, calculated from the rejection of neutral solutes (glucose and glycerol). This value agrees with pore size distribution determined by Hilal et al.[36] using atomic force microscopy.

3.1.2. Effective membrane charge density

NF membranes allow to separate ions by a combination of size exclusion and electrical effects. The electrical effects are closely related to the fixed charge uniformly distributed throughout the membrane active layer. The magnitude of this charge is quantified through the analysis of the 'effective membrane charge density' (X_d) parameter. The mechanism of membrane charge formation is related to the ionic concentration existing in the solution in contact with the membrane [28,37]. Physical determination of the magnitude of this parameter is not particularly well understood and it is normally obtained from the fitting between experimental and simulated ions rejection data using well known models [6,9,37-43]. It is highly desirable to develop

methods for predicting probable rejection of species based on quantifiable physicochemical properties of solutes and membranes [44]. Therefore, in this work the experimentally determined effective membrane charge density from measurements of the streaming potential has been used to predict NF sulfate and chloride ions rejection from high saline solutions.

The values of streaming potential for the model brines are collected in Table 2, obtained according to the procedure described in section 2.2. No significant differences are observed according to the average and standard deviation values calculated for triplicate measurements. Thus the average of the streaming potential data was considered for the calculation of the corresponding zeta potential (ζ) value using the Helmholtz-Smoluchowsky equation (Eq. 2). The membrane surface charge density (σ) values were determined through the Gouy-Chapmann equation (Eq. 3) using the calculated Debye length (κ^{-1}) (Eq. 4) for each of the brine compositions. Subsequently, membrane surface charge density was converted to concentration units (X_d) by using Eq. 5, which assumes that the membrane surface charge is uniformly distributed in the void volume of cylindrical pores [45,46].

$$\zeta = \frac{\frac{dV_{streaming}}{dP}\mu k_{solution}}{\varepsilon_0 \varepsilon_r} \qquad (2)$$

$$\sigma = \frac{2\varepsilon_0 \varepsilon_r \mathrm{K} k_B T}{ze} \sinh\left(\frac{ze\zeta}{2k_B T}\right) \qquad (3)$$

$$\mathrm{K}^{-1} = \sqrt{\frac{\varepsilon_0 \varepsilon_r RT}{2F^2 I}} \qquad (4)$$

$$X_d = \frac{2\sigma}{r_p F} \qquad (5)$$

As expected, the magnitude of charge density increased with increasing salt concentration due to the electrostatic adsorption [6,9,37-43,47]. Up to our knowledge here we report the first data of measured effective charge density X_d at saline concentrations as high as those found in water desalination brines.

3.1.3. Concentration polarization

In the pressure-driven liquid-phase membrane processes, such as NF, solutes and particles in the feed are convected towards the membrane with the solvent. The accumulation of retained species close to the membrane is known as concentration polarization which can be represented by a concentration gradient adjacent to the membrane [48]. The mass transfer coefficient (k) for each ion has been determined using the dimensionless correlation shown in equation 6 (also applied by Silva et al. [49] working with the same flat sheet cross flow cell SEPA CF from Osmonics) and considering the specific properties of the ion in solution.

$$Sh = 0.3125 \cdot Re^{0.57} Sc^{1/3} \tag{6}$$

The effect of concentration polarization in the modeling has been calculated as follows,

$$\frac{C_{0_i} - C_{p_i}}{C_{F_i} - C_{p_i}} = \exp\left(\frac{J_v}{k_i}\right) \tag{7}$$

being C_{0_i} the concentration at the membrane surface and C_{F_i} the feed concentration.

3.1.4. Membrane permeability measurement

Different models (Hagen-Poiseuille, Jonson and Boesen) have been proposed for the description of the volumetric flux through a NF membrane. They basically express the fundamental Darcy's law (flux proportional to pressure gradient) with an empirical proportionality constant, the permeability [50]. The volumetric flux is

related to the effective pressure gradient, that takes into account the applied pressure and the osmotic pressure difference as described by Eq.8.

$$J_v = L_p \cdot (\Delta P - \Delta \pi) \quad (8)$$

$\Delta\pi$ accounts for the influence of concentration polarization

$$\Delta \pi = \pi_0 - \pi_p \quad (9)$$

being π_0 the osmotic pressure corresponding to the concentration at the feed side membrane surface and π_p the osmotic pressure in the permeate side.

The osmomolality of different solutions with similar concentration to desalination brines was experimentally measured using a Crioscopic osmometer (CamLab, Löser), as shown in Fig. 2. Due to the fact that sulfate concentration remains almost constant, experimental values of osmomolality were fitted to sodium chloride concentration, achieving a correlation for the range of concentrations in feed-membrane side and another correlation for permeate concentrations.

The osmotic pressure was calculated through the cryoscopic temperature as given by equations (10) and (11),

$$\xi = \frac{\left(T_f^* - T_f\right)}{1.86} \cdot 1000 \quad (10)$$

$$\pi = \frac{\left(T_f^* - T_f\right) \cdot \Delta H_f^* \cdot T}{V_{molar\ solvent} \cdot T_f \cdot T_f^*} \left[\frac{R_{pressure}}{R}\right] \quad (11)$$

Experimental data of pure water flux showed a good linearity with the transmembrane pressure in the range from 500 kPa to 2000 kPa (regression coefficient R^2=0.99) and the obtained value of the membrane permeability to pure

water L_{pw} = 3.96·10^{-11} m Pa^{-1} s^{-1} (293 K) is very similar to the value reported by Nghiem and Hawkes [51] L_{pw}=3.75·10^{-11} m Pa^{-1} s^{-1} for the same membrane NF270 (Dow Filmtec). Working with saline solutions, the solution permeability decreased at increasing values of the ionic strength, although the relationship with the operating pressure is kept always linear, as it is shown in Fig. 3.

This behavior was previously observed by other authors [10,14,52]. A similar trend was observed by Otero et al [53], who found that solution permeability decreased exponentially with the initial salt concentration. In the present study, the variation of the membrane permeability L_p with saline concentration of the solution has been described by an exponential expression (Fig. 4).

3.2. Salts rejection

3.2.1. Effect of operating pressure

Fig. 5 depicts the results of sulfate, sodium and chloride rejection by the NF270 membrane as a function of the operating pressure. The rejection of the three ions increased with increasing operating pressure. Water flux also increases when the operating pressure increases, but the ion flux can be electrically and/or sterically hindered, resulting in a dilution effect in the permeate [54]. Therefore this effect causes lower ion concentration in the permeate and consequently the ion rejection might be higher. For the lower chloride/sulfate molar ratio used in this study, α=1.7, chloride rejection increases from -1.8% to 17.2%, sulfate rejection slightly changes from 95.2% to 95.9% and sodium rejection increments from 52.7% to 60.4% in the range of operating pressures from 500 kPa to 2000 kPa. Whereas for the higher molar ratio, α=13.6, chloride rejection varies from 1.7% to 10.1%, sodium rejection from 12.0% to 17.0% in the same range of operating pressure, and sulfate rejection

reaches its lowest value of 75.5% at the operating pressure of 500 kPa. In summary, sulfate rejection was in the range 76-96% while chloride rejections were between -2% and 17% in the studied range of pressures and saline concentrations.

3.2.2. Effect of the initial chloride concentration and ionic strength

In the studied conditions the ions rejection follows a similar trend with the initial chloride concentration than with the ionic strength, due to the influence of the former variable on the solution ionic strength. Donnan exclusion mechanism plays a major role in the rejection of inorganic solutes [55]. Negative chloride rejection is an often observed phenomenon that occurs with NF membranes applied to separation of mixtures of salts and large charged organic molecules and also when dealing with mixed monovalent-multivalent salts; it happens that the monovalent salt rejection is often negative [56,57]. Perry and Linder [58] explained for the first time this phenomenon and showed that the apparent negative rejection arised from the effect of the Donnan distribution of the salt between the solution and the membrane. Besides, increasing the ionic strength or the initial concentration of chloride reduces the retention ability of the membranes due to the lower influence of Donnan exclusion [59]. In this case, NF270 is a negatively charged membrane, therefore sodium ions (counter-ions) are attracted, while chloride and sulfate (co-ions) are repelled. This effect facilitates the transport of sodium ions through the membrane to the permeate side, and to maintain the electroneutrality condition, co-ions (sulfate and chloride) have to cross the membrane as well. Chloride permeation is higher than sulfate permeation due to chloride having lower ionic charge (less electrostatic repulsion) and lower ionic radius (less steric hindrance). This is the reason that makes sulfate rejection higher than chloride rejection. Fig. 6 shows that the rejection of sodium ions decreases with increasing ionic strength as a result of the increase of

sodium concentration in the permeate. Due to the fact that chloride rejection is no affected by increasing the ionic strength, more sulfate ions have to be transported through the membrane to the permeate phase in order to maintain the electroneutrality condition. Therefore, this explains the decrease of sulfate rejection with increasing ionic strength.

The sulfate rejection by NF270 membrane decreases from 95.9% to 81.3% with increasing the initial concentration of chloride from 0.2 to 1.2M for the operating pressure of 2000 kPa, and from 95.2% to 75.5% in the same range of initial chloride concentration and operating pressure of 500 kPa. The effect of operating pressure has been explained in the previous section 3.2.1.

3.3. Modeling of ionic rejection

In this work the Donnan Steric Pore Model (DSPM) has been used to describe the nanofiltration results (permeate flux and ions rejection) of multicomponent model brines using NF270 membrane. This model was firstly proposed by Bowen and Mukhtar [38], and then revised in Bowen and Mohammad [39]. Bandini and Vezzani [37] extended this model taking into account the dielectric exclusion (DE) phenomenon as an additional electrostatic partitioning effect, but they concluded that in the case of NaCl-Na_2SO_4 mixtures, dielectric exclusion was no relevant in determining ionic rejections and satisfactory agreement with experimental results was obtained both through DSPM and DSPM&DE model. The same analysis was done in the present study and the same conclusion was achieved: dielectric exclusion is no relevant in determining ionic rejections in high concentrated NaCl-Na_2SO_4 mixtures. However, in the case of working with more complex salt solutions containing for example calcium or magnesium salts, dielectric exclusion effect should be taken into account [37].

In the DSPM model, the transport equations of ions through the membrane are based on the extended Nernst–Planck equation, accounting for ion diffusion, electromigration and convection in the membrane pores; the hindered nature of diffusion and convection of the species inside the membrane pores is also considered. Ion partitioning at the interfaces between the membrane and the external liquid phases was taken into account through two separation mechanisms: steric hindrance and Donnan equilibrium. Therefore, the mathematical model of mass transport in this NF operation accounts for: (a) concentration polarization at the feed side; (b) equilibrium partitioning of the species at the feed/membrane interface; (c) solute transport through the membrane pores by a combination of convection, diffusion and electromigration and, (d) equilibrium partitioning of species at the membrane/permeate interface. Besides, the proposed NF model includes the mass balances to the NF cell, in order to obtain the description of the retentate. The fundamental equations of the model are detailed in Table 3.

The membrane is characterized by three parameters that are needed in order to predict the permeate concentration with the NF transport model: membrane pore radius (r_p), effective membrane thickness (δ) and effective membrane charge density (X_d). As mentioned in the previous section 3.1.1 the value of the pore radius was taken from literature and the effective membrane thickness was obtained from the analysis of SEM images. The membrane charge originates from the dissociation of ionisable groups at the membrane surface and within the membrane pore structure. Former literature [43,60,61] reported values of the "effective membrane charge density" (X_d) obtained from the best fitting of the experimental rejection vs total flux data. Other studies have measured the streaming potential to calculate membrane charge density working with low concentrated single salts solutions (concentration 2

orders of magnitude lower than brines) and with different NF membranes [46,47,62,63]. However, in this work we developed an experimental approach to obtain this parameter from experimental measurements of the streaming potential with highly saline concentrated solutions simulating desalination brines as described in section 3.1.2.

The mathematical equations were solved using the software Aspen Custom Modeler (AspenTech). It is known that concentration polarization increases with increasing concentration of salt solution when the system works at constant volumetric permeate flux. In this work, however, the polarization contribution has been analyzed and at the highest concentrations (α = 10.2 and 13.6) the influence of concentration polarization is negligible mainly due to the observed decrease in water flux. On the other hand, the influence of concentration polarization is higher at lower concentrations (α = 1.2 and 5.1) because of the higher water flux measured at high operation pressure and both conditions (Fig.3) . The effect of the concentration polarization effects on the modeling of ions rejection is plotted in Fig. 9b, validating the previous discussion.

The extended Nernst-Planck equation accounts for convection (pressure gradient), diffusion (concentration gradient) and electromigration (electric potential gradient) [64]. The electromigration term describes the migration as a result of an electric field. In the case of nanofiltration there is no external electric current but the electromigration term is due to the ions charge and difference of ions concentration across the membrane. Therefore, according to this definition it would be expected that its contribution to the flux of ions across the membrane would be lower than when an external electric field is applied, as in the case of electrodialysis. Next, the contribution of each transport mechanism to the ionic flux is analyzed. Because co-

ions are excluded from the membrane and counter-ions are attracted (due to the Donnan effect), the concentration of co-ions in the membrane is lower than that for counter-ions. Consequently, calculations of the contribution of each transport mechanism to the electrolyte transport will be performed with co-ions that are the limiting species to the overall electrolyte transport through the membrane [64]. Therefore, the contribution of the individual transport mechanisms to chloride and sulfate flux (J_{si}) towards the permeate side has been calculated (Tables 4 and 5).

Considering the contributions to the transport through the membrane of both co-ions, diffusion is the mechanism that governs the transport in this strongly charged membrane [65] and the effective charge density of the membrane determines the contribution of each transport mechanism.

Analysis of the individual transport mechanisms for the case of chloride (Fig. 7.a-c) shows that the more negative the charge density of the membrane, the lower the contribution of electromigration, because as the more negatively charged the membrane is the stronger the repulsion of chloride [55]. Conversely, the higher the charge density of the membrane is, the greater the contribution of the diffusive transport [65]. The diffusion is directly related to the concentration gradient, and due to the increase in the repulsion of chloride when the membrane is more negatively charged, the concentration gradient between membrane and permeate is higher. The contribution of the convective mechanism is directly related to the pressure gradient. As shown in Table 4, the contribution of convective transport increases with applied pressure.

With regards to the contributions of the different mechanisms to the transport of sulfate (Fig.8 a-c), the following behavior was observed, i) by increasing the molar ratio chloride/sulfate, or by increasing chloride concentration, the rate of

electromigration that contributes to sulfate transport follows the same trend as for the transport of chloride. However, the contribution of electromigration shows lower values than for the case of chloride, because sulfate is a divalent ion and therefore the repulsion exerted by the membrane is higher than for chloride [29]; ii) diffusion contribution to the transport of sulfate is almost constant as the sulfate concentration gradient does not vary with increasing chloride concentration in solution; iii) regarding the percentage contribution of the convective transport of sulfate, this percentage increases as the pressure gradient rises from 500 kPa to 2000 kPa.

Once the transport of ions through the membrane has been explained, simulated and experimental ions rejection data are compared as function of the operating pressure. Fig. 9b presents the experimental rejection of sulfate, sodium and chloride (symbols) together with simulated data (solid lines) as function of operating pressure. Simulated results with concentration polarization are in very good agreement with the experimental ions rejection data, with average standard deviation values of 2% for sulfate, 2% for sodium and 3% for chloride, thus, the model and parameters reported in this work, satisfactorily describe the behavior of the rejection of the ionic species (chloride, sulfate and sodium) with good accuracy. The simulated data of volumetric flux also show a reasonable agreement with the experimental values (Fig. 9a), and the model predicts the flux decline observed as the salt concentration increased.

4. CONCLUSIONS

The effectiveness of NF for sulfate/chloride separation in highly concentrated saline solutions has been experimentally and theoretically studied in this work. The membrane NF270 has proved to be very effective providing sulfate rejection in the

range 75-96% and chloride rejections between -2 and 11%. By increasing the salt concentration (NaCl) the retention ability of the membranes was reduced due to the decrease in Donnan effect. This is the reason that explains the reduction in sulfate rejection at increasing chloride concentration.

The design of the integrated membrane process requires of a reliable mathematical model that enables prediction of the behavior of NF stage under variable conditions of brine composition and operating pressure. The Donnan Steric Pore Model (DSPM) with experimentally determined parameters: effective pore radius (r_p); thickness of the membrane effective layer (δ) and effective membrane charge density (X_d), offers a good description of the experimental ionic rejection as function of operating pressure, providing the tools for process design and optimization.

Notation

A membrane surface (m^2)

C concentration (mol m^{-3})

C_1 concentration inside the membrane at feed/membrane interface (mol m^{-3})

C_2 concentration inside the membrane at membrane/permeate interface (mol m^{-3})

C_F feed mole concentration (mol m^{-3})

C_P permeate mole concentration (mol m^{-3})

C_R retentate mole concentration (mol m^{-3})

C_{eq} equivalent concentration (mol m^{-3})

D_∞ difussivity of ions (m^2 s^{-1})

D_p hindered diffusivity (m^2 s^{-1})

e electronic charge (C)

F Faraday constant (C/mol)

J_S molar solute flux (mol m^{-2} s^{-1})

J_V total volume flux (m s^{-1})

k_B Boltzmann constant (J/K)

$k_{solution}$ conductivity of electrolyte solution (S/m)

K_c convective hindrance factor, dimensionless

K_d diffusive hindrance factor, dimensionless

L_p solution membrane permeability (m s^{-1} Pa^{-1})

L_{pw} water membrane permeability (m s^{-1} Pa^{-1})

N_A Avogadro number

Q_F feed flow (m^3/s)

Q_P permeate flow (m^3/s)

Q_R retentate flow (m^3/s)

r_i Stoke radius of ion (m)

r_p effective pore radius (m)

$\mathcal{R}$ ion rejection, dimensionless

R universal constant of gases (J mol^{-1} K^{-1})

$R_{pressure}$ universal constant of gases (Pa m^3 K^{-1} mol^{-1})

T operation temperature (K)

T_f solution fusion temperature (K)

T_f^* water fusion temperature (K)

V_{molar} water molar volume (m^3 mol^{-1})

$V_{streaming}$ streaming potential (V)

X_d effective membrane charge density (mol m^{-3})

z ionic valence, dimensionless

Greek letters

α ratio chloride concentration vs sulfate concentration ($\alpha=[Cl^-](M)/[SO_4^{2-}](M)$)

δ thickness of the membrane effective layer (m)

ΔH_f^* water fusion latent heat (J mol^{-1})

$\Delta\pi$ osmotic pressure difference across the membrane (Pa)

ΔP applied pressure difference across the membrane (Pa)

$\Delta\psi_{Donnan}$ Donnan potential, dimensionless

ε_0 vacuum permittivity (C/m V)

ε_r dielectric constant of water, dimensionless

κ^{-1} Debye length (m)

ξ osmomolality (mosmol (kg H_2O)$^{-1}$)

ζ zeta potential (V)

λ relative solute size ($\lambda = r_i/r_p$), dimensionless

μ solution viscosity (kg/m s)

σ electrical charge on the membrane surface (C/m^2)

Φ steric partitioning coefficient, dimensionless

Subscripts

i ion

F feed

P permeate

R retentate

Acknowledgements.

This work has been financially supported by projects CTQ2008-0690, ENE2010-15585 and CTM2011-23912 (co-financed by ERDF Funds). The authors would like to acknowledge SADYT, S.A. for providing assistance for this work.

REFERENCES

[1] I. Muñoz, A.R. Fernández-Alba, Reducing the environmental impacts of reverse osmosis desalination by using brackish groundwater resources, Water Res. 42 (3) (2008) 801-811.

[2] D. Zarzo, E. Campos, Project for the development of innovative solutions for brines from desalination plants, Deswater 31(2011) 206-217.

[3] P. Palomar, I.J. Losada, Desalination impacts on the marine environment, The Marine Environment: Ecology, Management and Conservation (2011) 1.

[4] A. Pérez-González, A.M. Urtiaga, R. Ibáñez, I. Ortiz, State of the art and review on the treatment technologies of water reverse osmosis concentrates, Water Res. 46 (2)(2012) 267–283.

[5] R. Ibáñez, A. Pérez-González, P. Gómez, A.M. Urtiaga, I. Ortiz, Acid and base recovery from softened reverse osmosis (RO) brines. Experimental assessment using model concentrates, Desalination 309 (2013) 165-170.

[6] D.L. Oatley, L. Llenas, R. Pérez, P.M. Williams, X. Martínez-Lladó, M. Rovira, Review of the dielectric properties of nanofiltration membranes and verification of the single oriented layer approximation, Adv. Colloid Interface Sci. 173 (2012) 1-11.

[7] S. Yüksel, N. Kabay, M. Yüksel, Removal of bisphenol A (BPA) from water by various nanofiltration (NF) and reverse osmosis (RO) membranes, J.Hazard.Mat. 263 (2) (2013) 307-310.

[8] B. Van der Bruggen, A. Koninckx, C. Vandecasteele, Separation of monovalent and divalent ions from aqueous solution by electrodialysis and nanofiltration, Water Res. 38 (2004) 1347-1353.

[9] D. Hu, Z-L. Xu, Y-M. Wei, Y-F. Liu, Poly(styrene sulfonic acid) sodium modified nanofiltration membranes with improved permeability for the softening of highly concentrated seawater, Desalination 336 (2014) 179-186.

[10] G. Bargeman, M. Steensma, A. ten Kate, J.B. Westerink, R.L.M. Demmer, H. Bakkenes, C.F.H. Manuhutu, Nanofiltration as energy-efficient solution for sulfate waste in vacuum salt production, Desalination 245 (2009) 460-468.

[11] J. Benavente , V. Silva, P. Prádanos, L. Palacio, A. Hernández, G. Jonson, Comparison of the volume charge density of nanofiltration membranes obtained from retention and conductivity experiments, Langmuir 26 (14) (2010) 11841-11849.

[12] J. Luo, Y. Wan, Effects of pH and salt on nanofiltration-a critical review, J. Memb. Sci. 438 (2013) 18-28

[13] J.M. Gozálvez-Zafrilla, A.Santafé-Moros, J.Carlos García-Díaz, Crossed mixture-process design approach to model nanofiltration rejection for non-dilute multi-ionic solutions in a given range of solution compositions, Desalination 315 (2013) 61-69.

[14] D.L. Oatley-Radcliffe, S.R. Williams, M.S. Barrow, P.M. Williams, Critical appraisal of current nanofiltration modelling strategies for seawater desalination and further insights on dielectric exclusion, Desalination 343 (2014) 154-161.

[15] N. Pages, A. Yaroshchuk, O.Gilbert, J.L. Cortina, Rejection of trace ionic solutes in nanofiltration: Influence of aqueous phase composition, Chem. Eng. Sci. 104 (2013) 1107-1115.

[16] A. Yaroshchuk, X. Martínez-Lladó, L. Llenas, M. Rovira, J. de Pablo, Solution-diffusion- film model for the description of pressure-driven trans-membrane

transfer of electrolyte mixtures: one dominant salt and trace ions, J. Memb. Sci. 368 (2011) 192-201.

[17] V. Silva, A. Martin, F. Martinez, J. Malfeito, P. Prádanos, L. Palacio, A.Hernández, Electrical characterization of NF membranes. A modified model with charge variation along the pores, Chem. Eng. Sci. 66 (2011) 2898-2911.

[18] N. Hilal, H. Al-Zoubi, A.W. Mohammad, N.A. Darwish, Performance of nanofiltration membranes in the treatment of synthetic and real seawater, Sep. Sci. Technol. 42 (2007) 493-515.

[19] B. Van der Bruggen, J. Kim, Nanofiltration of aqueous solutions: Recent developments and progresses, Advanced Materials for Membrane Preparation, Bentham Science Publisher (2012) 228-247.

[20] C.R. Martinetti, A.E. Childress, T.Y. Cath, High recovery of concentrated RO brines using forward osmosis and membrane distillation, J. Memb. Sci. 331(2009) 31-39.

[21] G. Artug, I. Roosmasari, K. Richau, J. Hapke, A comprehensive characterization of commercial nanofiltration membranes, Sep. Sci. Technol. 42(2007) 2947-2986.

[22] M. Dalwany, N.E. Benes, G. Bargeman, D. Stamatialis, M. Wessling, Effect of pH on the performance of polyamide/polyacrylonitrile based thin film composite membranes, J. Memb. Sci. 372(2011) 228-238.

[23] S.N. Diop, M.A. Diallo, C.K. Diawara, D. Cot, Intrinsic properties and performances of NF270 and XLE membranes for water filtration, Water Sci. Technol. 11(2) (2011) 186-193.

[24] Y.L. Lin, P.C. Chiang, E.E. Chang, Removal of small trihalomethane precursors from aqueous solution by nanoflitration, J. Hazard. Mater. 146 (2007) 20-29.

[25] M. Mänttäri, A. Pihlajamäki, M. Nyström, Effect of pH on hydrophilicity and charge and their effect on the filtration efficiency of NF membranes at different pH, J. Memb. Sci. 280 (2006) 311-320.

[26] A. Simon, L-D. Nghiem, P. Le-Clech, S.J. Khan, J.E. Drewes, Effects of membrane degradation on the removal of pharmaceutically active compounds (PhACs) by NF/RO filtration processes, J. Memb. Sci. 340 (2009) 16-25.

[27] A. Simon, W.E. Price, L.D. Nghiem, Influence of formulated chemical cleaning reagents on the surface properties and separation efficiency of nanofiltration membranes, J. Memb. Sci. 432 (2013) 73-82.

[28] A.E. Childress, M. Elimelech, Effect of solution chemistry on the surface charge of polymeric reverse osmosis and nanofiltration membranes, J. Memb. Sci. 119 (1996) 253-268.

[29] J.M.M. Peeters, M.V.H. Mulder, H. Strathmann, Streaming potential measurements as a characterization method for nanofiltration membranes, Colloids and Surfaces A: Physicochemical and Engineering Aspects 150 (1999) 247-259.

[30] A.E. Childress, M. Elimelech, Relating nanofiltration membrane performance to membrane charge (Electrokinetic) characteristics, Environ. Sci. Technol. 34 (2000) 3710-3716.

[31] S. Deón, P. Dutournié, P. Bourseau, Modeling Nanofiltration with Nernst-Planck Approach and Polarization Layer, AIChE Journal 53 (8) (2007)1952-1969.

[32] C. Mazzoni, S. Bandini, On nanofiltration Desal-5 DK performances with calcium chloride-water solutions, Sep. Purif. Techn. 52 (2006) 232-240.

[33] L. Meihong, Y. Sanchuan, Z. Yong, G. Congjie, Study on the thin-film composite nanofiltration membrane for the removal of sulfate from concentrated salt aqueous: Preparation and performance, J. Membr. Sci. 310 (2008) 289-295.

[34] N. Hilal, H. Al-Zoubi, A.W. Mohammad, N.A. Darwish, Nanofiltration of highly concentrated salt solutions up to seawater salinity, Desalination 184 (2005a) 315-326.

[35] M.J. Ariza, A. Cañas, J. Benavente, J, Electrical and surface chemical characterizations of the active layer of composite polyamide/polysulphone nanofiltration commercial membranes, Surf. Interface Anal. 30 (2000) 425-429.

[36] N. Hilal, H. Al-Zoubi, A.W. Mohammad, N.A. Darwish, Characterisation of nanofiltration membranes using atomic force microscopy, Desalination (2005b) 187-199.

[37] S. Bandini, D. Vezzani, Nanofiltration modeling: the role of dielectric exclusion in membrane characterization, Chem. Eng. Sci. 58 (2003) 3303-3326.

[38] W.R. Bowen, H.Mukhtar, Characterisation and prediction of separation performance of nanofiltration membranes, J.Memb. Sci. 112 (1996) 263-274.

[39] W.R. Bowen, A.W. Mohammad. Diafiltration by Nanofiltration: Prediction and Optimization, AIChE Journal 44 (1998) 1799-1812.

[40] W.R. Bowen, J.S. Welfoot, P.M. Williams, Linearizared transport model for nanofiltration: Development and Assessment, AIChE Journal 48 (2002) 760- 773.

[41] W.R. Bowen, J.S. Welfoot, Modelling of membrane nanofiltration-pore size distribution effects, Chem. Eng. Sci. 57 (2002) 1393-1407.

[42] W.R. Bowen, B. Cassey, P. Jones, D.L. Oatley, Modelling the performance of membrane nanofiltration-application to an industrially relevant separation, J. Memb. Sci. 242 (2004) 211-220.

[43] A. W. Mohammad, N. Hilal, H. Al-Zoubi, N.A. Darwish, Prediction of permeate fluxes and rejections of highly concentrated salts in nanofiltration membranes, J. Memb. Sci. 289 (2007) 40-50.

[44] A.R.D. Verliefde, E.R. Cornelissen, S.G.J. Heijman, E.M.V. Hoek, G.L. Amy, B. Van der Bruggen, J.C. van Dijk, Influence of solute-membrane affinity on Rejection of Uncharged Organic Solutes by Nanofiltration Membranes, Environ. Sci. Technol. 43 (2009) 2400-2406.

[45] M.D. Afonso, G. Hagmeyer, R. Gimbel, Streaming potential measurements to assess the variation of nanofiltration membranes surface charge with the concentration of salts solutions, Sep. Purif. Technol. 22-23 (2001) 529-541.

[46] A.I. Cavaco Morão, A. Szymczyk, P. Fievet, A.M Brites Alves, Modelling the separation by nanofiltration of a multi-ionic solution relevant to an industrial process, J. Memb. Sci. 322 (2008) 320-330.

[47] S. Deón, A. Escoda, P. Fievet, A transport model considering charge adsorption inside pores to describe salts rejection by nanofiltration membranes. Chem. Eng. Sci. 66 (2011) 2823-2832.

[48] A.G. Fane, Module design and operation, in: A.I. Schäfer, A.G. Fane, T.D. Waite (Eds.), Nanofiltration-Principles and Applications, Elsevier, Amsterdam (2005) pp.67-88.

[49] V. Silva, V. Geraldes, A.M. Brites Alves, L.Palacio, P.Prádanos, A. Hernández, Multi-ionic nanofiltration of highly concentrated salt mixtures in the seawater range. Desalination 277 (2011) 29-39.

[50] B. Van der Bruggen, M. Mänttäri, M. Nyström, Drawbacks of applying nanofiltration and how to avoid them: A review, Sep. Purif. Technol. 63 (2008) 251-263.

[51] L.D. Nghiem, S. Hawkes, Effects of membrane fouling on the nanofiltration of pharmaceutically active compounds (PhACs): Mechanisms and role of membrane pore size, Sep. Purif. Technol. 57 (2007) 176-184.

[52] C. Rodrigues, A.I. Cavaco-Morao, M.N. de Pinho, V. Geraldes, On the prediction of permeate flux for nanofiltration of concentrated aqueous solutions with thin-film composite polyamide membranes, J.Memb, Sci., 346 (2010) 1-7.

[53] J.A. Otero, G. Lena, J.M. Colina, P. Prádanos, F. Tejerina, A. Hernández, Characterisation of nanofiltration membranes. Structural analysis by the DSP model and microscopical techniques, J. Memb. Sci., 279 (2006) 410-417.

[54] J. Fang, B. Deng, Rejection and modeling of arsenate by nanofiltration: Contributions of convection, diffusion and electromigration to arsenic transport, J. Memb. Sci. 453 (2014) 42-51.

[55] A.R.D. Verliefde, E.R. Cornelissen, S.G.J. Heijman, J.Q.J.C. Verbeck, G.L. Amy, B. Van der Bruggen, J.C. van Dijk, The role of electrostatic interactions on the rejection of organic solutes in aqueous solutions with nanofiltration, J. Memb. Sci. 322 (2008) 52-66.

[56] J. Gilron, N. Gara, O.Kedem, Experimental analysis of negative salt rejection in nanofiltration membranes, J. Memb. Sci. 185 (2001) 223-236.

[57] W.R. Bowen, J.S. Welfoot, Modelling the performance of nanofiltration membranes, in: A.I. Schäfer, A.G. Fane, T.D. Waite (Eds.), Nanofiltration-Principles and Applications, Elsevier, Amsterdam, 2005, pp.119-146.

[58] M. Perry, C. Linder, Intermediate reverse osmosis ultrafiltration (RO/UF) membranes for concentration and desalting of low molecular weight organic solutes, Desalination 71 (1989) 233-245.

[59] R. Jiraratananon, A. Sungpet, P. Luangsowan, Performance evaluation of nanofiltration membranes for treatment of effluents containing reactive dye and salt, Desalination 130 (2000) 177-183.

[60] S. Bandini, Modelling the mechanism of charge formation in NF membranes: Theory and application, J. Memb. Sci. 264 (2007) 75-86.

[61] R. Navarro, M.P. González, I. Saucedo, M. Avila, P. Prádanos, F. Martínez, A. Martín, A. Hernández, Effect of an acidic treatment on the chemical and charge properties of a nanofiltration membrane, J. Memb. Sci. 307 (2008) 136-148.

[62] A. Szymczyk, P. Fievet, Investigating transport properties of nanofiltration membranes by means of a steric, electric and dielectric exclusion model, J.Memb.Sci. 252 (2005) 77-88.

[63] A. Escoda, P. Fievet, S. Lakard, A. Szymczyk, S. Déon, Influence of salts on the rejection of polyethylene glycol by an NF organic membrane: Pore swelling and salting-out effects, J. Memb. Sci. 347 (2010) 174-182.

[64] P. Fievet, C. Labbez, A. Szymczyk, A. Vidonne, A. Foissy, J. Pagetti, Electrolyte transport through amphoteric nanofiltration membranes. Chem. Eng. Sci. 57 (2002) 2921-2931.

[65] A. Szymczyk, C. Labbez, P. Fievet, A. Vidonne, A. Foissy, J. Pagetti, Contribution of convection, diffusion and migration to electrolyte transport through nanofiltration membranes, Adv. Colloid Interface Sci. 103 (2003) 77-94.

Table 1. Average chemical characterization of the RO brines of three desalination plants: Cuevas de Almazora, Carboneras and Las Aguilas. Values of the standard deviation of the analytical techniques are given within brackets.

	Desalination plants		
Parameter	Cuevas de Almanzora	Carboneras	Las Aguilas
pH	7.9 (0.01)	8 (0.01)	9 (0.01)
Conductivity(μS/cm) es mili o micro)	34,300 (0.5)	95,500 (0.5)	96,160 (0.5)
Hardness (mg $CaCO_3$/L)	13,000 (0.04)	18,000 (0.14)	16,400 (0.09)
TDS (mg/L)	20,700 (0.5)	70,000 (0.5)	70,488 (0.5)
Chloride (mg/L)	7,279 (0.10)	37,955 (0.20)	38,887 (9.38)
Sulfate (mg/L)	8,465 (0.06)	7,243 (0.50)	5,316 (0.29)
Nitrate (mg/L)	447 (0.01)	0 (0.00)	1.8 (0.04)
Phosphate (mg/L)	0.3 (0.03)	0.025 (0.01)	-
Sodium (mg/L)	5,176 (0.24)	17,020 (0.29)	21,922 (5.85)
Magnesium (mg/L)	1,589 (0.47)	2,715 (0.40)	2,479 (0.14)
Calcium (mg/L)	1,828 (0.46)	796 (0.22)	791 (0.04)
Potassium (mg/L)	178 (0.59)	816 (0.51)	743 (0.25)
Carbonate (mg/L)	0 (0.00)	18 (0.00)	155 (0.00)
Bicarbonate (mg/L)	826 (0.07)	217 (0.04)	173 (0.07)

Table 2. Streaming potential, zeta potential and effective membrane charge density values determined after membrane immersion in model brines.

$\alpha = \frac{[Cl^-]}{[SO_4^{2-}]}$	NaCl *(M)*	$\frac{dV_{streaming}}{dP}$ *(mV/bar)*	Average $\frac{dV_{streaming}}{dP}$ *(mV/bar)*	ζ *(mV)*	X_d *(mol/m^3)*
1.70	0.14	-0.42±0.23	-0.4	-6.34	-265
5.10	0.42	-0.54±0.27			-459
10.20	0.85	-0.39±0.41			-649
13.60	1.13	-0.25±0.37			-750

.Table 3. Fundamental equations of the proposed NF model.

Mass balances

$$Q_F = Q_R + Q_P$$

$$C_{F_i} \cdot Q_F = C_{R_i} \cdot Q_R + C_{P_i} \cdot Q_P$$

$$Q_P = J_v \cdot A$$

$$J_v = L_p(\Delta P - \Delta \pi)$$

$$\sum_{i=1}^{n} z_i \cdot C_{R_i} = 0$$

$$C_{eq} = \frac{1}{2}\sum_{i=1}^{n} |z_i| C_{F_i}$$

a) Concentration polarization at the feed side

$$\frac{C_{0_i} - C_{p_i}}{C_{F_i} - C_{p_i}} = \exp\left(\frac{J_v}{k_i}\right)$$

b) Equilibrium partitioning of the species at the feed/membrane interface

$$\frac{C_{1_i}}{C_{0_i}} = \phi_i \exp\left[-z_i \Delta\psi_{Donnan}(0)\right]$$

c) Solute transport through the membrane

$$J_{s_i} = J_v K_{c_i} C_i - D_{p_i}\frac{dC_i}{dx} - z_i C_i D_{p_i}\frac{F}{RT}\frac{d\psi}{dx}$$

$$\frac{d\psi}{dx} = \frac{\sum_{i=1}^{n} z_i \frac{J_v}{D_{p_i}}[K_{c_i} C_i - C_{P_i}]}{\left(\frac{F}{RT}\right)\sum_{i=1}^{n} z_i^2 C_i}$$

$$J_{s_i} = J_v \cdot C_{P_i}$$

$$D_{p_i} = K_{d_i} \cdot D_{\infty_i}$$

Hindrance factors ($0 < \lambda \leq 0.8$)

$$K_{d_i} = 1.0 - 2.30\lambda_i + 1.154\lambda_i^2 + 0.224\lambda_i^3$$

$$K_{c_i} = 1.0 + 0.054\lambda_i - 0.988\lambda_i^2 + 0.441\lambda_i^3$$

d) Equilibrium partitioning of species at the membrane/permeate interface

$$\frac{C_{2_i}}{C_{P_i}} = \phi_i \exp\left[-z_i \Delta\psi_{Donnan}(\delta)\right]$$

Steric partitioning

$$\phi_i = (1-\lambda_i)^2 \qquad \lambda_i = \frac{r_i}{r_p}$$

Electroneutrality conditions

$$\sum_{i=1}^{n} z_i C_{P_i} = 0$$

$$\sum_{i=1}^{n} z_i C_i + \mathrm{X}_d = 0$$

Table 4. Contribution of diffusion, convection and electromigration mechanisms to chloride flux.

	P (kPa)	J_s**chloride** (mol m^{-2} s^{-1})	% Diffusion	% Convection	% Electromigration
α=1.7	500	1.92E-03	71%	11%	18%
	1000	3.01E-03	66%	13%	22%
	2000	5.30E-03	55%	16%	28%
α=5.1	500	3.18E-03	73%	14%	13%
	1000	5.31E-03	71%	14%	15%
	2000	9.40E-03	64%	16%	20%
α=10.2	500	3.04E-03	75%	17%	8%
	1000	5.87E-03	73%	17%	10%
	2000	1.12E-02	70%	18%	12%
α=13.6	500	2.83E-03	76%	17%	7%
	1000	5.81E-03	75%	18%	8%
	2000	1.14E-02	72%	18%	10%

Table 5. Contribution of diffusion, convection and electromigration mechanisms to sulfate flux.

	P (kPa)	J_s**sulfate** (mol m^{-2} s^{-1})	% Diffussion	% Convection	% Electromigration
α=1.7	500	8.11E-05	82%	11%	7%
	1000	1.41E-04	71%	17%	11%
	2000	4.01E-04	55%	27%	18%
α=5.1	500	6.37E-05	90%	7%	3%
	1000	9.02E-05	83%	12%	5%
	2000	1.77E-04	70%	20%	10%
α=10.2	500	5.65E-05	95%	4%	1%
	1000	7.37E-05	91%	8%	2%
	2000	1.13E-04	83%	14%	4%
α=13.6	500	5.00E-05	96%	4%	1%
	1000	6.51E-05	93%	6%	1%
	2000	9.42E-05	86%	12%	2%

.

Highlights

- Reverse Osmosis (RO) brines as source of valuable compounds
- Nanofiltration for RO brines conditioning before bipolar membrane electrodialysis
- High sulfate/chloride separation efficiency with NF270 membrane
- Donnan Steric Pore Model describes monovalent and divalent anions separation by NF

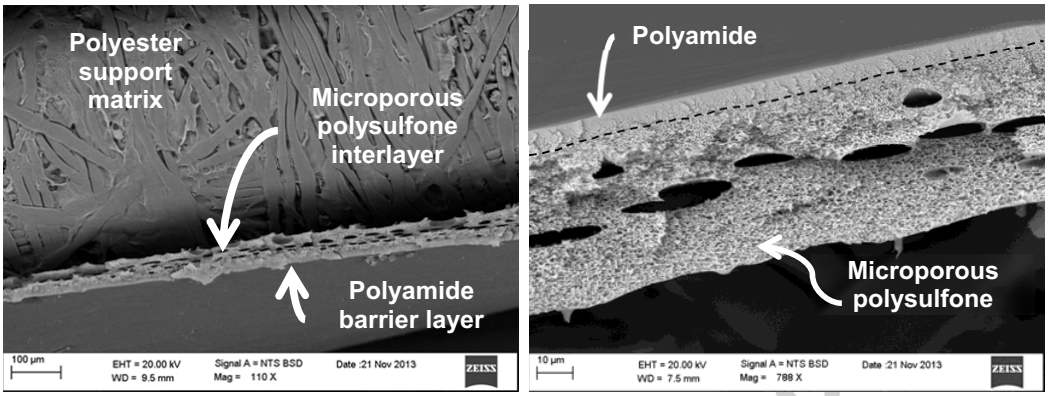

Fig. 1. SEM images of the NF270 membrane employed in this study.

.

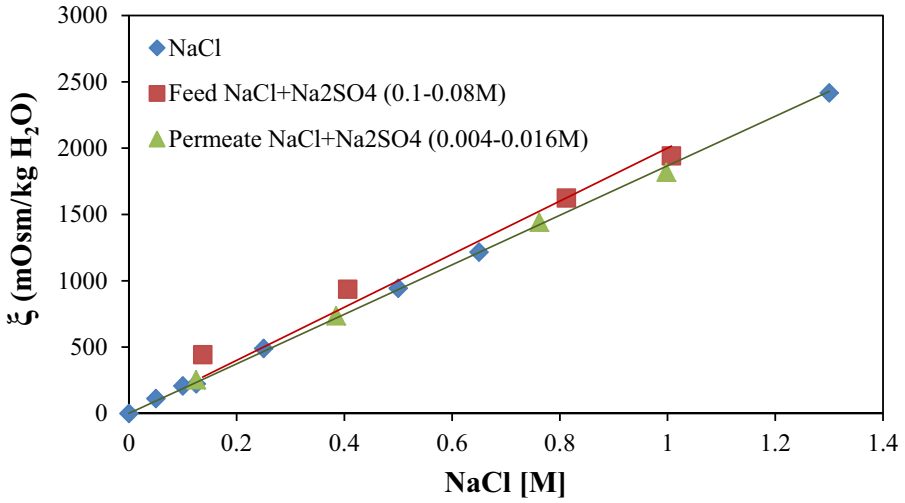

Fig. 2. Experimental linear correlations of osmomolality vs NaCl concentration. Linear fitting : feed solutions: ξ=2001*[NaCl] ; permeate solutions: ξ=1867*[NaCl].

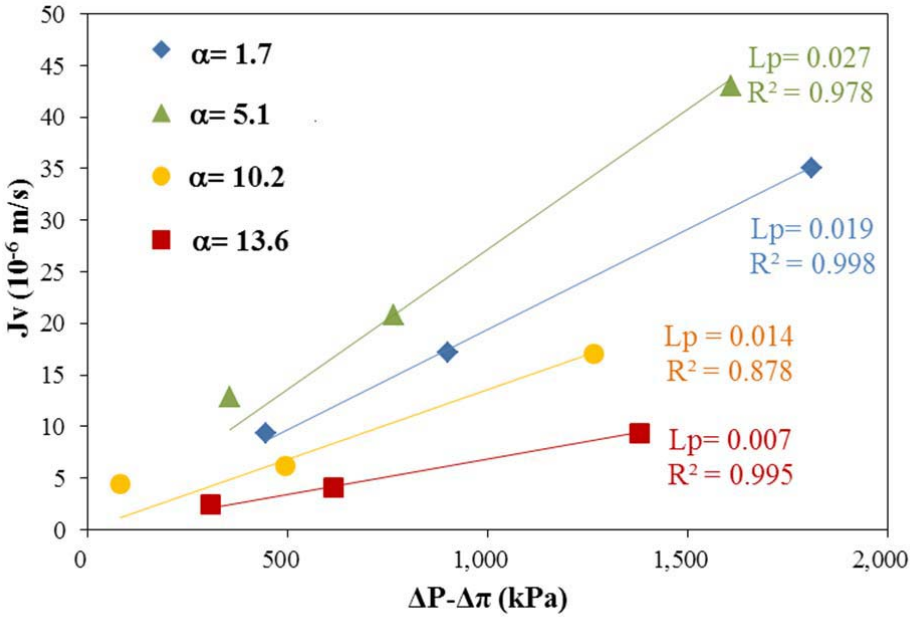

Fig. 3. Experimental flux data as a function of α and effective pressure. Linear fitting of solution permeability.

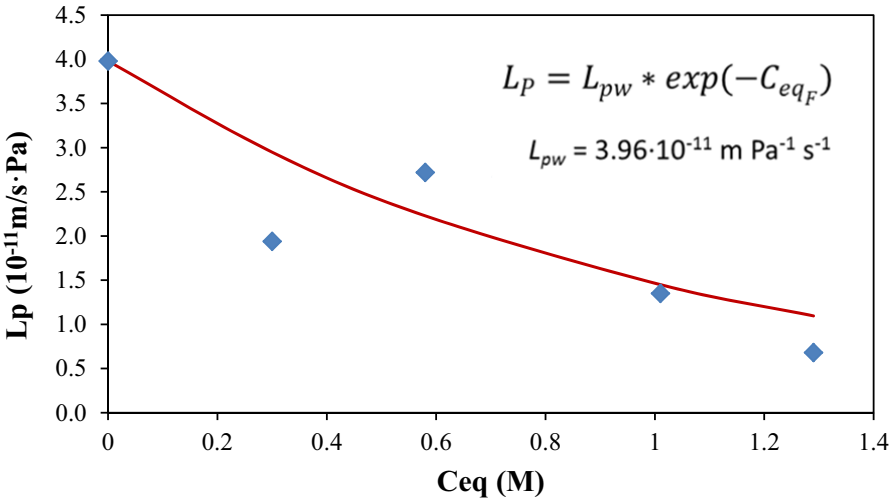

Fig. 4. Variation of the membrane permeability with brine saline concentration

Figure 5

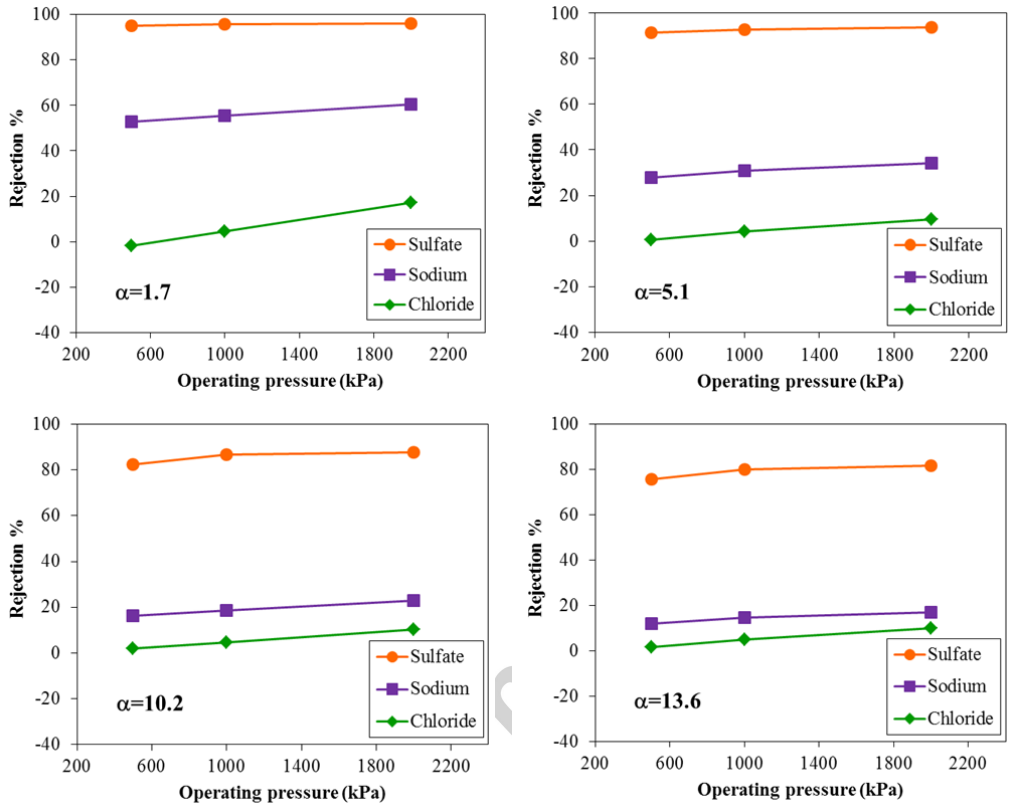

Fig. 5. Experimental ion rejection as a function of α (molar ratio Cl^-/SO_4^{2-}) and operating pressure

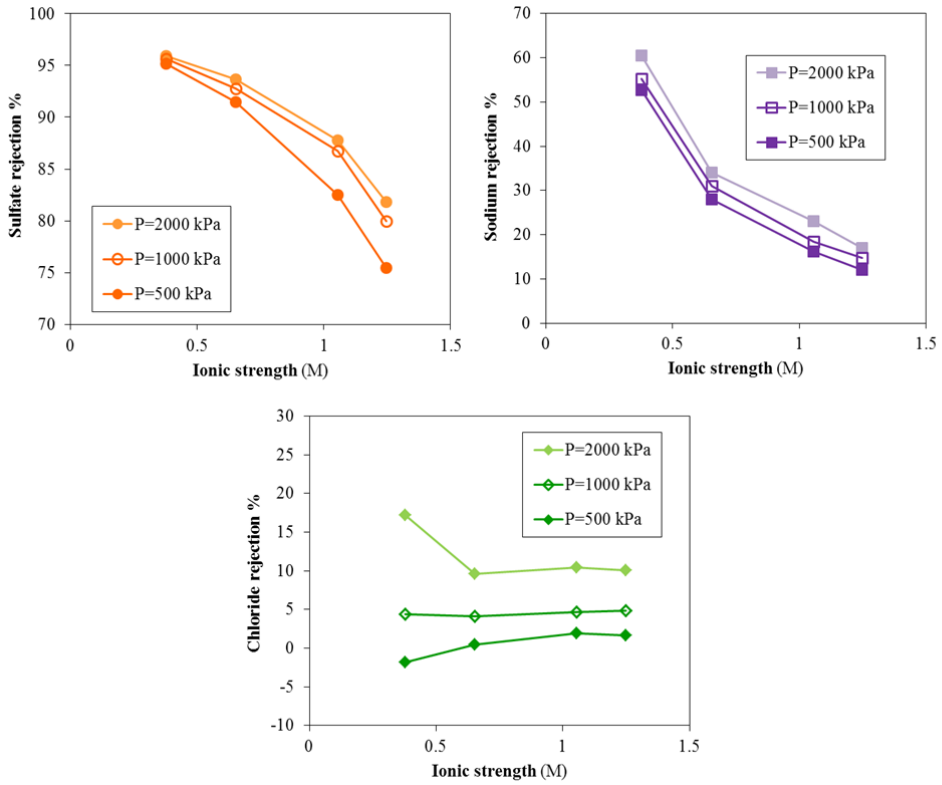

Fig. 6. Experimental results of sulfate, sodium and chloride rejection as function of ionic strength (pH value=6.3±0.3)

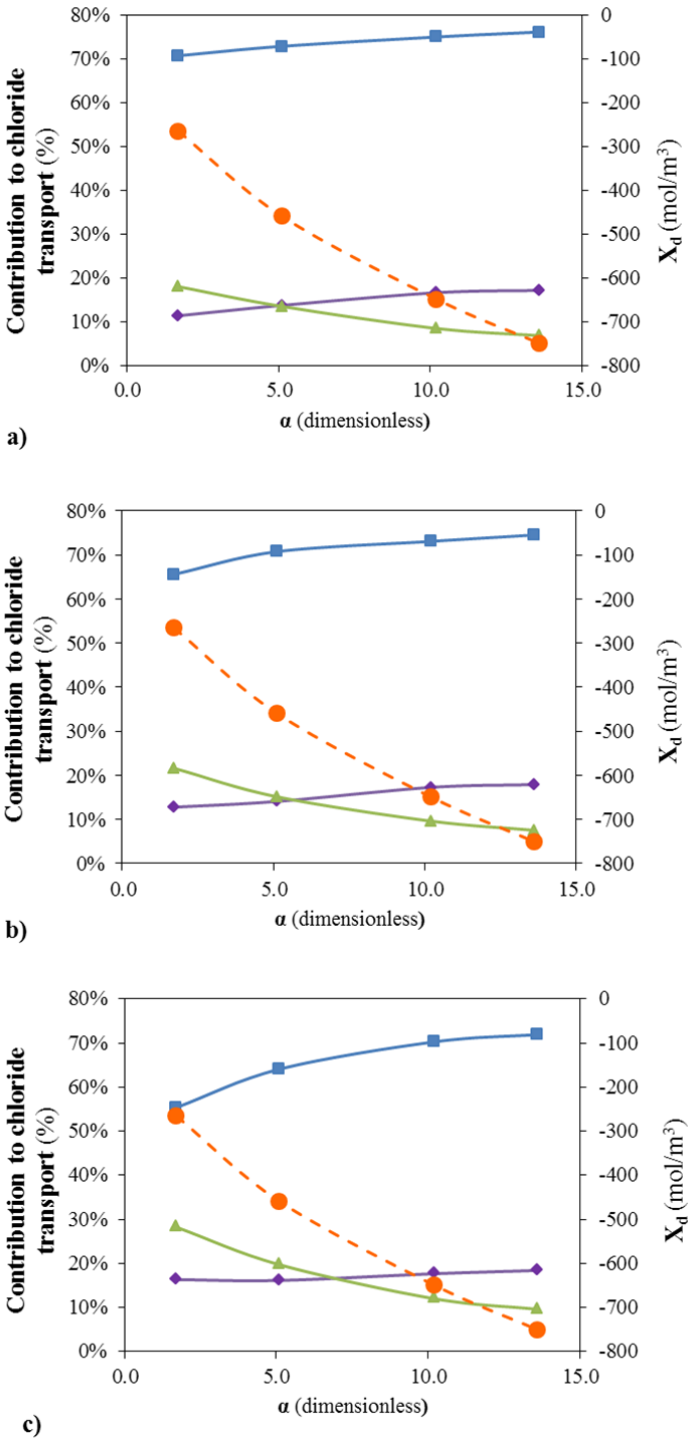

Fig. 7. Individual transport mechanisms of solute flux (Jsi) for chloride: diffussion( ), convection ( ) and electromigration ( ) as function of the molar ratio chloride/sulfate(α): **a)** 500kPa; **b)** 1000 kPa; **c)** 2000 kPa. Comparison to effective membrane charge density trend ( )

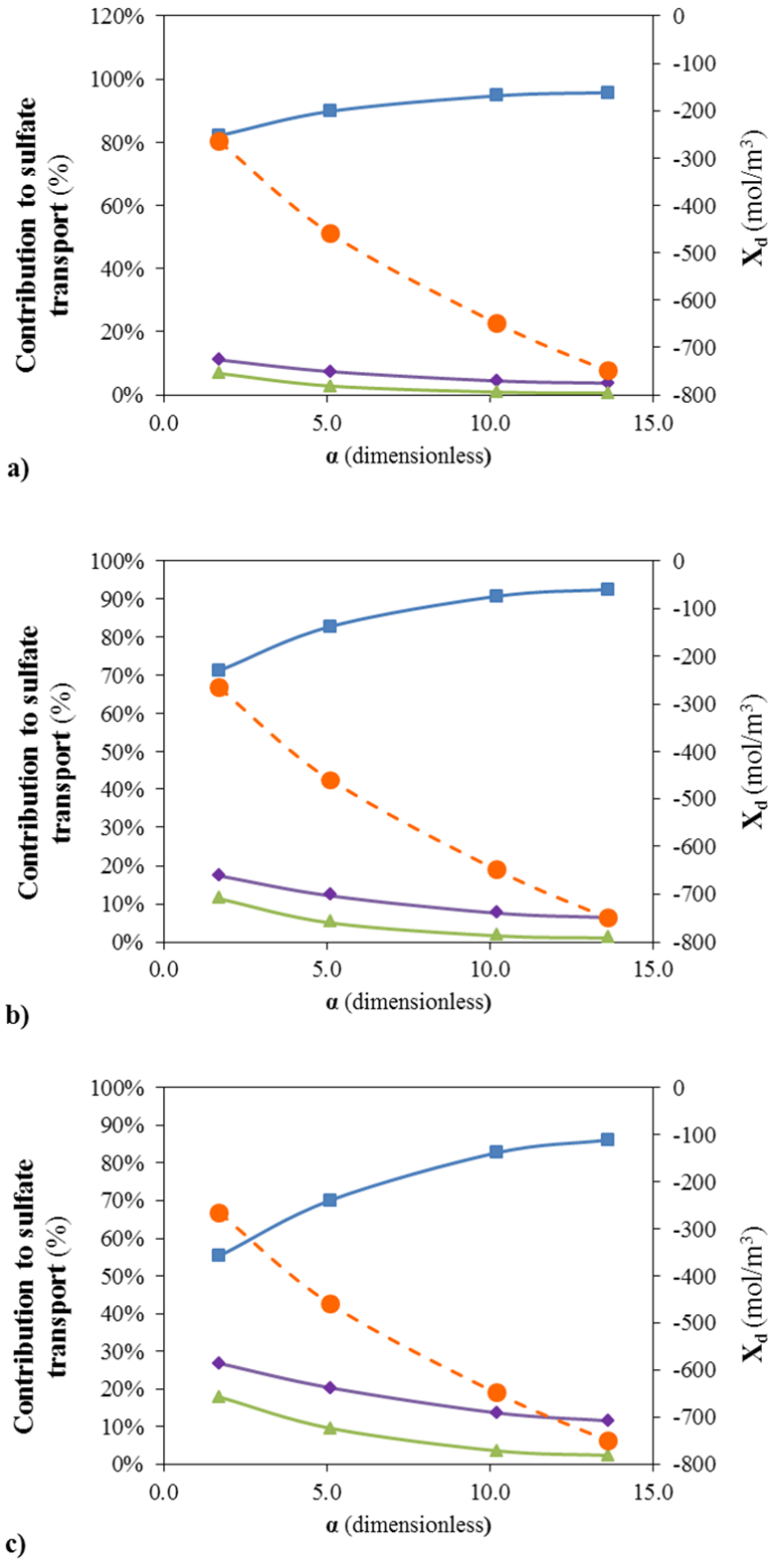

Fig. 8. Individual transport mechanisms of solute flux (Jsi) for sulfate: diffussion( ), convection ( ) and electromigration ( ) as function of molar ratio chloride/sulfate(α): **a)** 500kPa; **b)** 1000 kPa; **c)** 2000 kPa. Comparison to effective membrane charge density trend ( )

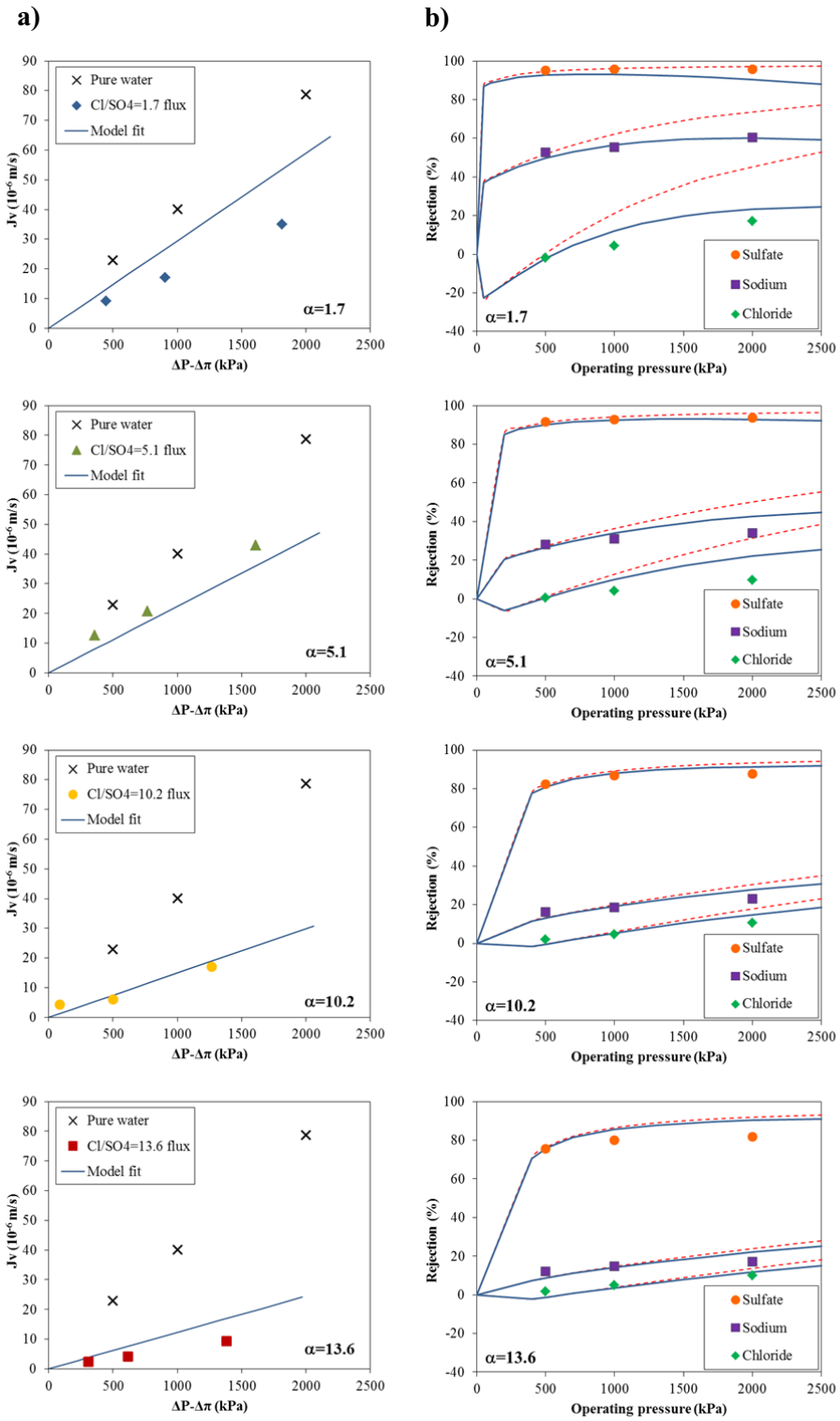

Fig. 9.a) Experimental flux data (symbols) and simulated flux (solid lines) and their comparison with the experimental pure water flux as a function of α and effective pressure. **b)** Experimental (symbols) and predicted (lines) ions rejection data as a function of α and operating pressure. Simulated results without concentration polarization (- - -) and with concentration polarization (———)